



UNIVERSIDAD REGIONAL AMAZÓNICA IKIAM
FACULTAD DE CIENCIAS DE LA TIERRA Y AGUA
CARRERA DE GEOCIENCIAS

**RESPUESTA DE LOS DESLIZAMIENTOS DE TIERRA A LA
DINÁMICA DE LA PRECIPITACIÓN, MEDIDA MEDIANTE RADAR
INTERFEROMÉTRICO DE APERTURA SINTÉTICA: UN CASO DE
ESTUDIO EN LA PARTE SUR DE LA DEPRESIÓN INTERANDINA
ECUADOR**

Proyecto de investigación previo a la obtención del Título de:

INGENIERO EN GEOCIENCIAS

AUTOR

FREDDY JAVIER LIMA BURI

Napo – Ecuador

2024



UNIVERSIDAD REGIONAL AMAZÓNICA IKIAM
FACULTAD DE CIENCIAS DE LA TIERRA Y AGUA
CARRERA DE GEOCIENCIAS

**RESPUESTA DE LOS DESLIZAMIENTOS DE TIERRA A LA
DINÁMICA DE LA PRECIPITACIÓN, MEDIDA MEDIANTE RADAR
INTERFEROMÉTRICO DE APERTURA SINTÉTICA: UN CASO DE
ESTUDIO EN LA PARTE SUR DE LA DEPRESIÓN INTERANDINA
ECUADOR**

Proyecto de investigación previo a la obtención del Título de:
INGENIERO EN GEOCIENCIAS

AUTOR: FREDDY JAVIER LIMA BURI
TUTOR: GABRIEL V. GAONA

Napo – Ecuador
2024

DECLARACIÓN DE DERECHO DE AUTOR, AUTENTICIDAD Y RESPONSABILIDAD

Yo, Freddy Javier Lima Buri, con documento de identidad N° 1150986113, declaro que los resultados obtenidos en la investigación que presento en este documento final, previo a la obtención del título de Ingeniero en Geociencias, son absolutamente inéditos, originales, auténticos y personales.

En virtud de lo cual, el contenido, criterios, opiniones, resultados, análisis, interpretaciones, conclusiones, recomendaciones y todos los demás aspectos vertidos en la presente investigación son de mi autoría y de mi absoluta responsabilidad.

Tena, 09 de febrero de 2024



Freddy Javier Lima Buri
1150986113

AUTORIZACIÓN DE PUBLICACIÓN EN EL REPOSITORIO INSTITUCIONAL

Yo, Freddy Javier Lima Buri, con documento de identidad N° 1150986113, en calidad de autor/a y titular de los derechos morales y patrimoniales del trabajo de titulación: **Respuesta de los deslizamientos de tierra a la dinámica de la precipitación, medida mediante radar interferométrico de apertura sintética: un caso de estudio en la parte sur de la Depresión Interandina Ecuador**, de conformidad con el Art. 114 del CÓDIGO ORGÁNICO DE LA ECONOMÍA SOCIAL DE LOS CONOCIMIENTOS, CREATIVIDAD E INNOVACIÓN, reconozco a favor de la Universidad Regional Amazónica Ikiam una licencia gratuita, intransferible y no exclusiva para el uso no comercial de la obra, con fines estrictamente académicos.

Así mismo autorizo a la Universidad Regional Amazónica Ikiam para que realice la publicación de este trabajo de titulación en el Repositorio Institucional de conformidad a lo dispuesto en el Art. 144 de la Ley Orgánica de Educación Superior.

Tena, 09 de febrero de 2024



Freddy Javier Lima Buri

1150986113

CERTIFICADO DE DIRECCIÓN DE TRABAJO DE TITULACIÓN

Certifico que el trabajo de titulación: “Respuesta de los deslizamientos de tierra a la dinámica de la precipitación, medida mediante radar interferométrico de apertura sintética: un caso de estudio en la parte sur de la Depresión Interandina Ecuador” en la modalidad de: artículo, fue realizado por Freddy Javier Lima Buri, bajo mi dirección.

El mismo ha sido revisado en su totalidad y analizado por la herramienta de verificación de similitud de contenido; por lo tanto, cumple con los requisitos teóricos, científicos, técnicos, metodológicos y legales establecidos por la Universidad Regional Amazónica Ikiam, para su entrega y defensa.

Tena, 09 de febrero de 2024



Gabriel Vicente Gaona Gaona

C.I: 1104176563

DEDICATORIA

A mis hermanos, en especial a Manuel Lima, Roberth Lima, José Luis Lima, por el apoyo incondicional que me brindaron. A mis padres, por los consejos y la confianza que depositaron en mí.

A mis amigos, por hacer de esta etapa universitaria una gran experiencia.

A mis profesores por la paciencia, dedicación y pasión que mostraron en las aulas. Gracias por la sed de conocimientos que me supieron impartir.

Y como olvidarme de ti, gracias Jia, gracias por ser mi compañera incondicional.

AGRADECIMIENTO

Agradecimientos sinceros a:

Mi tutor, MSc. Gabriel Gaona, por la confianza, el apoyo y el conocimiento que me impartió.

A todos los docentes de la Carrera de Geociencias por despertar mi curiosidad por este maravilloso mundo de las Geociencias.

A la Agencia Europea Espacial, Agencia Japonesa de Exploración Aeroespacial, proyecto ARIA por proveer imágenes de radar de forma libre. A los desarrolladores de los softwares: ISCE2, MintPy and Biwavelet por las herramientas para la realización de este trabajo.

TABLA DE CONTENIDO

DECLARACIÓN DE DERECHO DE AUTOR, AUTENTICIDAD Y RESPONSABILIDAD	2
AUTORIZACIÓN DE PUBLICACIÓN EN EL REPOSITORIO INSTITUCIONAL	3
DEDICATORIA	6
AGRADECIMIENTO	7
TABLA DE CONTENIDO	8
ÍNDICE DE TABLAS	9
ÍNDICE DE GRÁFICOS O FIGURAS	9
RESUMEN	10
ABSTRACT	11
1. INTRODUCTION	1
2. METHODOLOGY	3
2.1 Study area description:	3
2.2 InSAR time series analysis	4
2.2.1 Interferograms generation	4
2.2.2 InSAR time series analysis	5
2.2.3 Landslides identification	5
2.2.4 Selection of displacement pixels and rainfall time series	5
2.3 Time-frequency analysis by continuous wavelet analysis	6
3. RESULTS	8
3.1 Interferograms generated	8
3.2 InSAR velocity analysis	8
3.3 Pixels selection	12
3.4 Continuous wavelet transform for rainfall and nonlinear term displacement time series	12
3.4.1 Continuous wavelet analysis for rainfall	12
3.4.2 Continuous wavelet analysis for displacement nonlinear term	13
3.4.3 Coherence wavelet analysis	14
4. DISCUSSION	15
4.1 InSAR limitation	15
4.2 Relationship between InSAR displacement and rainfall	16
5. CONCLUSION	16
6. BIBLIOGRAPHY	

ÍNDICE DE TABLAS

Table 1. Comparison between landslides identified in this work and previous inventories.....	12
--	----

ÍNDICE DE GRÁFICOS O FIGURAS

Figure 1. Study area description, a) Tectonic setting, b) geological setting and c) topography.....	4
Figure 2. Landslides identification and velocity map period 2007-2011.....	10
Figure 3. Landslides identification and velocity map period 2016-2022.....	11
Figure 4. Landslides annual velocity average. a-b) Annual velocity landslides #1 and #14. b-d) Annual velocity landslides #1 and #12. e) Rainfall anomalies for landslide #9.....	12
Figure 5. Pixels selection for time series analysis. a) and b) Cumulated displacement for landslides #1 and #12 respectively	13
Figure 6. Continuous wavelet analysis for rainfall time series.....	14
Figure 7. Continuous wavelet analysis for landslide displacement time series.....	15
Figure 8. Correlation measure between landslide #1 displacement and rainfall by continuous wavelet coherence.....	16
Figure 9. Correlation measure between landslide #12 displacement and rainfall by continuous wavelet coherence.....	16

Revista a presentar: Landslides, Journal of the International Consortium on Landslides

RESUMEN

Los deslizamientos de tierra de baja velocidad presentan un movimiento descendente continuo e imperceptible para el ser humano que ponen en peligro a las poblaciones aledañas. Localizar la extensión espacial de estos y su respuesta a las variaciones de la precipitación es vital para predecir el riesgo en una zona. El Radar interferométrico de apertura sintética (InSAR) es una técnica geodésica útil para analizar el comportamiento temporal-espacial de los deslizamientos de tierra. El desplazamiento de los deslizamientos derivado de InSAR representa las fluctuaciones estacionales desencadenadas por las estacionalidades de la precipitación. En este trabajo se utilizó la técnica InSAR para identificar deslizamientos de tierra en la parte sur de la Depresión Interandina de Ecuador y correlacionar su desplazamiento estacional con la precipitación utilizando el análisis wavelet. Se identificaron 20 deslizamientos de tierra en el periodo 2007 a 2011 y de 2016 a 2022. Tres deslizamientos muestran una velocidad media que oscila entre 7 milímetros por año y 26,5 milímetros por año. El análisis wavelet muestra que los deslizamientos de tierra se correlacionan con las precipitaciones en periodos/escalas interanuales, anuales y multianuales. Los resultados sugieren que las respuestas rápidas de desplazamiento de los deslizamientos de tierra pueden estar relacionadas con eventos de alta precipitación, mientras que las respuestas anuales y multianuales podrían estar relacionadas con las propiedades mecánicas del suelo o con procesos de aguas subterráneas.

Palabras clave: Deslizamientos, InSAR, análisis wavelet, precipitación, Depresión Interandina.

ABSTRACT

Slow-moving landslides exhibit continuous, human-imperceptible downslope motion risking human settlements. Localizing the landslide's spatial extension and response under rainfall variation is vital for predicting the hazard for an area. Synthetic aperture radar interferometry (InSAR) time series is a useful geodetic technique to analyze temporal-spatial landslide behavior. Landslide displacement derived from InSAR represents seasonal, fast and slow motion fluctuation triggered by rainfall stationarities. Here, InSAR was used to identify landslides in the southern part of the Neogen Inter Andean Depression of Ecuador and correlate landslides' seasonal displacement with rainfall using wavelet analysis. Twenty landslides were identified from 2007 to 2011 and 2016 to 2022. Three landslides exhibit InSAR average velocity ranging from 7 millimeters per year to 26.5 millimeters per year. The wavelet analysis shows landslides correlate with rainfall in infra-annual, annual, and multiannual periods/scales. The results suggest that fast landslide displacement responses are related to high rainfall events, while annual and multiannual responses might relate to soil mechanic properties or groundwater processes.

Keywords: Landslides, InSAR, wavelet analysis, rainfall, Inter Andean Depression.

1. INTRODUCTION

The study area (Fig. 1b), the southern part of the Inter Andean Depression home to about 400 thousand people distributed in cities such as Riobamba, Alausi, Tixan, Guamote, as well as other assets such as the Pan-American Highway, has been affected by landslides (e.g., Vasconez et al. (2023)). Catastrophic landslides can collapse suddenly due to trigger factors such as earthquakes (Schuster et al., 1996), and extreme rainfall events (Temple & Rapp, 1972), claiming lives (Froude & Petley, 2018). In contrast, slow-moving landslides rarely fail catastrophically (Hendron & Patton, 1987). Slow-moving landslides move downslope at rates of mm/year, they can occur in the vicinity of cities (Soto et al., 2017) damaging human infrastructure (Nappo et al., 2019).

Due to their progressive movement, and seasonal response to precipitation, slow-moving landslides can be better studied in order to explore their kinematic response to external factors. Varnes, (1978) classifies landslides by type of material involved and movement rate. In this work, as well as in Bekaert et al. (2020), a slow-moving landslide is a mass movement process that shows continuous downslope movements < 1.6 m/y (Hung et al., 2014). Under the latter definition, in the remainder of this work landslide term will be used instead of slow-moving landslides.

Landslides, its spatial-temporal evolution, and kinematic response to precipitation have been encompassed through different approaches. Field techniques including inclinometers, extensometers, and Global Positioning (GPS) System stations have been used by Soralump et al. (2021) to obtain accurate landslide slope deformation measures as response to precipitation. Nevertheless, these techniques give low-spatial information of the landslide process and involve human supervision for their correct functioning (Casagli et al., 2023), which can be a highly resource-consuming activity. Remote sensing techniques (space-borne or ground-based) (Casagli et al., 2023) such as Interferometric Synthetic Aperture Radar (InSAR) can give accurate surface deformation measurements in order of mm of wide areas.

InSAR is a space-borne remote sensing technique that measures surface deformation using Synthetic Aperture Radar (SAR) images (Simons & Rosen, 2007). SAR sensors use microwaves to acquire data, which have cloud-penetration capability and image

the earth's surface during night and day because they are active sensors (Ferretti et al., 2007). Although SAR images cover wide surfaces, the temporal gap of data acquisition has barred a proper study of spatial-temporal evolution phenomena such as landslides. In recent years, space agencies such as The European Space Agency and the Japan Aerospace Exploration Agency have launched the Sentinel 1A/B and ALOS 1-2 missions respectively, to obtain detailed spatial-temporal evolution of the earth process. For instance, temporal resolutions for Sentinel 1A/B and ALOS 1 are 6 and 46 days respectively.

InSAR has been widely used in earth science to measure surface deformation related to landslides events (Hilley et al., 2004), volcanic eruptions (Gregg et al., 2022), and postseismic deformation. Champenois et al., (2017) and Scheingross et al., (2013) used InSAR in an uplifting tectonic environment to assess fault zone control over landslides distribution and size. Research as Handwerger et al. (2019) studies landslides kinematic response to a change from drought to extreme rainfall events. Mackey et al., (2009) and Mackey & Roering, (2011) assessed the role of the landslides over sediment flux into river networks and hillside erosion. Lag time response of landslides displacement to precipitation has been carried out by Handwerger et al., (2013) and Cohen-Waeber et al. (2018).

Assessing the relationship between landslide displacement and rainfall is not trivial work, since landslide displacement does not show a linear displacement trend (Corominas et al., 2005). The wavelet analysis allows us to extract frequency components of the time series and identify where those exist in the temporal domain. The continuous wavelet transform (CWT) and wavelet coherence (WCT) approaches have been implemented respectively to assess landslides displacement periodicities and relationship with trigger factors (Tomás et al., 2016; Vallet et al., 2016).

In this work, the InSAR time series technique was used to identify landslides in the southern part of the Inter Andean Depression between two time periods from December 2006 to March 2011 and November 2015 to November 2021. Landslide displacement time series patterns and their relationship with rainfall were assessed by the wavelet analysis approach.

2. METHODOLOGY

2.1 Study area description:

The study area is located in the Inter Andean Depression (IAD) (Fig. 1b). The IAD is a Neogen depression between The Western Cordillera and Real Cordillera developed by the coalition plate border between the Nazca Plate under the Continental South America plate (Fig. 1a). The oblique subduction setting has developed a north-east moving sliver, the North Andean Sliver (NAS), which is moving northeastward at 9 mm/yr (Nocquet et al., 2014). The NAS east border corresponds to the active Chingual, Cosanga Pallatanga Puna Fault system (CCPP) (Nocquet et al., 2014; Alvarado et al., 2016).

Geographically, the study encompasses a polygon between latitudes -1.6° S and -2.14° S, and longitudes 79° W and 78.5° W along the Pan-American highway. The elevation ranges between 2000 m to 4000 m (Fig. 1c). The IAD presents two rainy seasons from February-May and October-November, as well as, the driest period ranging from June-September and a moderate one around December (Vuille et al., 2000). The precipitation rate varies between 800 and 1500 mm/y (Vuille et al., 2000; Crespo et al., 2011).

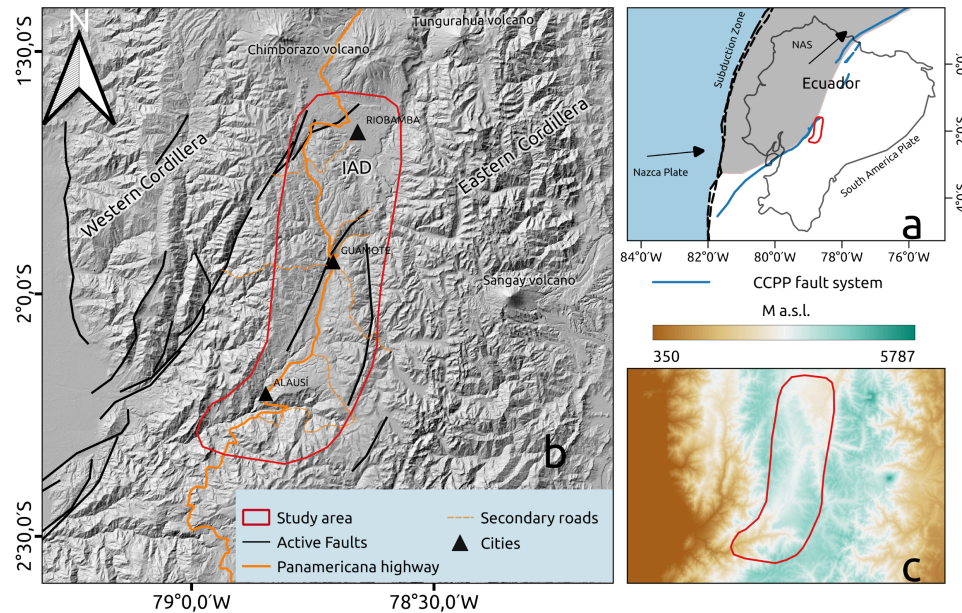


Figure 1: a) Shows the tectonic framework where the Nazca plate obliquely subducts the South American plate and the CCPP (Chingual Cosanga Pallatanga Puna) fault system, which corresponds to the border east of NAS. b) Main geological structures and active faults dataset from (Styron & Pagani, 2020; Baize et al., 2020). c) Elevation gradient from 30-meters SRTM DEM.

Realizado por: Javier Lima

2.2 InSAR time series analysis

InSAR measures earth surface displacement by exploiting phase differences between a first SAR image (related reference image) and a second SAR image gathered over the same area at different times. SAR image cell resolution is related to two dimensions: along-track direction (satellite flight direction or azimuth direction) and across-track direction (ground range direction). InSAR measures direction is related to the line of sight (LOS), which is an imaginary line between the SAR sensor and ground target, therefore, targets moving toward and away from the satellite are considered as positive and negative motion respectively.

InSAR techniques (e.g. DInSAR approach) have been widely used in earth science for measuring single deformation events such as fault slips by seismic events (Massonnet et al., 1993; Champenois et al., 2017), and volcanic activities (Gregg et al., 2022). In contrast to single deformation events, large-area ground displacement such as landslides, which are mainly driven by precipitation (Bogaard & Greco, 2016) occur over long periods (Mackey et al., 2009) thus, it can not be measured by a single interferogram, which is why the time series InSAR method is required. InSAR time

series analysis consists of two main steps: 1) interferogram generation and 2) InSAR time series analysis.

2.2.1 Interferograms generation

SAR images provided by L-band ALOS/PALSAR and C-band Sentinel 1AB spaceborne missions with 46 and 6 days temporal resolution respectively, were used for interferogram generation. The interferograms generated from ALOS/PALSAR images between 2007 and 2011 were performed by using the ALOS1 stack processor workflow (Fattahi et al., 2017) implemented in the InSAR Scientific Computing Environment (ISCE) (Rosen et al., 2012). A detailed process for interferogram generation is shown in Bürgmann et al. (2000). Between December 2015 and January 2022, interferograms generated from Sentinel 1AB images by the Advanced Rapid Imaging and Analysis (ARIA), Center for Natural Hazards project (Buzzanga et al., 2020) were used. PALSAR images acquired in L-band frequency (~ 23.5 cm wavelength) are better suited than C-band frequency (~ 5.6 cm wavelength) to map landslides over vegetated areas (Lu et al., 2010; Liu et al., 2021).

2.2.2 InSAR time series analysis

Repeat-pass SAR images generally decorrelate with time, hence the longer the temporal baseline (time separation between SAR acquisitions) the noisier the interferograms. Decorrelation phenomenon is related to changes in the surface backscatter characteristics over time (Hanssen, 2001). Over dense vegetation areas correlation loss is driven by changes in physical and chemical properties over time (Zebker & Villasenor, 1992). Therefore, the correlation measures the quality of the interferogram, expressed in terms of SAR coherence ranging from 0 to 1 (low to high quality).

Time series analysis was performed using the Small Baseline Subset technique (SBAS) (Berardino et al., 2002), implemented as The Miami INsar Time-series software in Python (MintPy) by (Yunjun et al., 2019). A coherence threshold of 0.6 was applied for interferogram selection. InSAR measurements are relative in space, thus stable reference pixels were located close to landslides. The products obtained from InSAR time series analysis are average velocity and displacement time series, where

average velocity is estimated as the slope of the best fitting line to the displacement time series (Yunjun et al., 2019).

2.2.3 Landslides identification

Landslides were identified by InSAR velocity and displacement maps. Landslides motion can be recognized against background deformation because landslides show localized deformation areas (Handwerger et al., 2022) (Fig. 2a and Fig. 3a). Additionally, InSAR velocity maps were projected on an ALOS/PALSAR twelve-meter resolution DEM (available at <https://search.asf.alaska.edu/#/>) to corroborate InSAR velocity signals with landslide topographic features (e.g., lateral margins, crown) (Scheingross et al., 2013).

2.2.4 Selection of displacement pixels and rainfall time series

To select pixels that represent landslide displacement, only pixels showing cumulative displacement sum between the 75th and 98th percentile were selected (Fig. 4) highlights the selected pixels.

Daily rainfall data with $0,05^\circ$ (~ 5.3 km) spatial resolution were obtained from Climate Hazards Group InfraRed Precipitation with Station data (CHIRPS) (available at https://data.chc.ucsb.edu/products/CHIRPS-2.0/global_daily/netcdf/p05/) in netCDF format (Funk et al., 2014).

2.3 Time-frequency analysis by continuous wavelet analysis

Wavelet transform as well as Fourier transform extracts frequency components of a signal (e.g. geophysical time series). Fourier transform analysis is a good choice for analyzing stationary time series, in which statistical properties (e.g. mean, standard deviation) are constant over time, however, Fourier transform gives no information about the temporal evolution of the frequencies (Lau & Weng, 1995). Geophysical time series are not stationary signals (Grinsted et al., 2004), therefore a process that extracts frequencies of a time series and also analyzes how frequencies change over time is required. The continuous wavelet transform (CWT) provides a time-frequency representation of the time series. The Morlet wavelet function, which consists of a plane wave modulated by a Gaussian, was used.

$$\Psi_0(t) = \pi^{-1/4} e^{i\omega_0 t} e^{-t^2/2} \quad (1)$$

where i is the imaginary unit, t represents non dimensional time parameter, and $\omega_0 = 6$ represent nondimensional frequency (Torrence & Compo, 1998). Given a discrete, equal time spaced (δt) time series $x(t)$ of length T the continuous wavelet transform of $x(t)$ is defined as (Grinsted et al., 2004):

$$W_x(s, \tau) = \sqrt{\frac{\delta t}{s}} \sum_{t=0}^{T-1} x(t) \Psi_0^* \left(\frac{(t-\tau)\delta t}{s} \right) \quad (2)$$

where $*$ denote the complex conjugate. By varying s (scale factor) one can stretch (2) to capture low frequencies or compress it to capture high frequencies components, while the function is shifted through the signal by τ (position factor) (Lau & Weng, 1995).

In this study, the continuous wavelet transform (CWT) was used to analyze InSAR displacement and rainfall time series. The CWT's purpose is to identify localized intermittent periodicities of an individual time series (Tomás et al., 2016). As a result, the CWT gives a 2-D dimension (time and frequencies/periods axes) spectrum image that shows regions with high and low power in the time-frequency space.

To measure the strength of the covariation between two time series $x(t)$, and $y(t)$ one can use the coherence wavelet transform (WTC) define as (Torrence & Compo, 1998) and (Grinsted et al., 2004):

$$R_{x,y}^2(s, \tau) = \frac{|\langle s^{-1} W_{x,y}(s, \tau) \rangle|^2}{\langle s^{-1} |W_x(s, \tau)|^2 \rangle \langle s^{-1} |W_y(s, \tau)|^2 \rangle} \quad (3)$$

where $W_{x,y}(s, \tau)$ is the cross wavelet transform define as (Grinsted et al., 2004):

$$W_{x,y}(s, \tau) = W_x(s, \tau) * W_y(s, \tau) \quad (4)$$

where $*$ denotes the complex conjugate. The $\langle \dots \rangle$ is the smoothing factor in both scale s and time τ .

The WTC was used to measure the relationship between displacement and rainfall signals; more details about WTC can be found in (Grinsted et al., 2004). The WTC 2-D spectrum shows areas in the time-frequency space where both time series show common periodicities. The CWT is ranging from 0 to 1, values of 1 means perfect high linear correlation between time series, otherwise areas close to 0 have no correlation. Readers are encouraged to visit (Torrence & Compo, 1998) for a step-by-step guide of continuous wavelet transform, practical applications in climate (Grinsted et al., 2004) and landslides (Tomás et al., 2016).

The CWT requires equal time step measurements across time series. For InSAR time series displacement this means an equal temporal baseline between acquisitions. Although Sentinel 1 has a regular 6-day repeat interval, gaps occur due to low coherence interferograms dropped in the InSAR time series generation or missed images concerning technical problems on the satellites (e.g. high Doppler centroid on SAR data). A six-day, equal-space displacement time series was obtained by using linear interpolation method.

After interpolation procedure displacement time series was decomposed in linear and non-linear components. The linear component is computed by means of a linear least squares fitting, while the non-linear component is the difference between displacement time series and the linear component (Tomás et al., 2016). Daily rainfall was accumulated every 6 days to match the displacement time series.

Statistical hypothesis test assesses how wavelet power or coherence exceeds a background noise (Schulte, 2019). For geophysical phenomena such as El Niño–Southern Oscillation, landslides displacement a red noise process is a good choice for background noise spectrum, in fact the wavelet power of geophysical time series is compared against red noise spectrum ($P(k)$) (Torrence & Compo, 1998).

$$P(k) = \frac{1-\alpha^2}{1+\alpha^2-2\alpha\cos\left(\frac{2\pi k}{N}\right)} \quad (5)$$

where α is the autocorrelation coefficient calculated from the analyzed time series and $k = 0 \dots N/2$ is the frequency index. The continuous wavelet transform for the Morlet function has been implemented by (Tarik et al., 2018) in R environment as biwavelet software.

3. RESULTS

3.1 Interferograms generated

Eighteen L-band SAR images acquired by ALOS/PALSAR satellite along the ascending orbit (satellite moving south-north looking east) track 110 and 111 were used to perform 167 interferograms from 2007 to 2012. ARIA project provided 483 interferograms along ascending orbit track 18.

3.2 InSAR velocity analysis

Fourteen landslides were identified during the periods 2007-2011 and 2016-2022; landslide motion is related in LOS direction (Fig. 2) and (Fig. 3). Landslide slopes facing westward show positive values meaning that landslides are moving toward the satellite. Since landslides only can move downslope direction, InSAR LOS direction measures the horizontal component of downslope motion. Landslide slopes facing eastward show negative velocity in LOS direction meaning that landslides are moving away from the satellite. The latter was assumed as a landslide downslope motion.

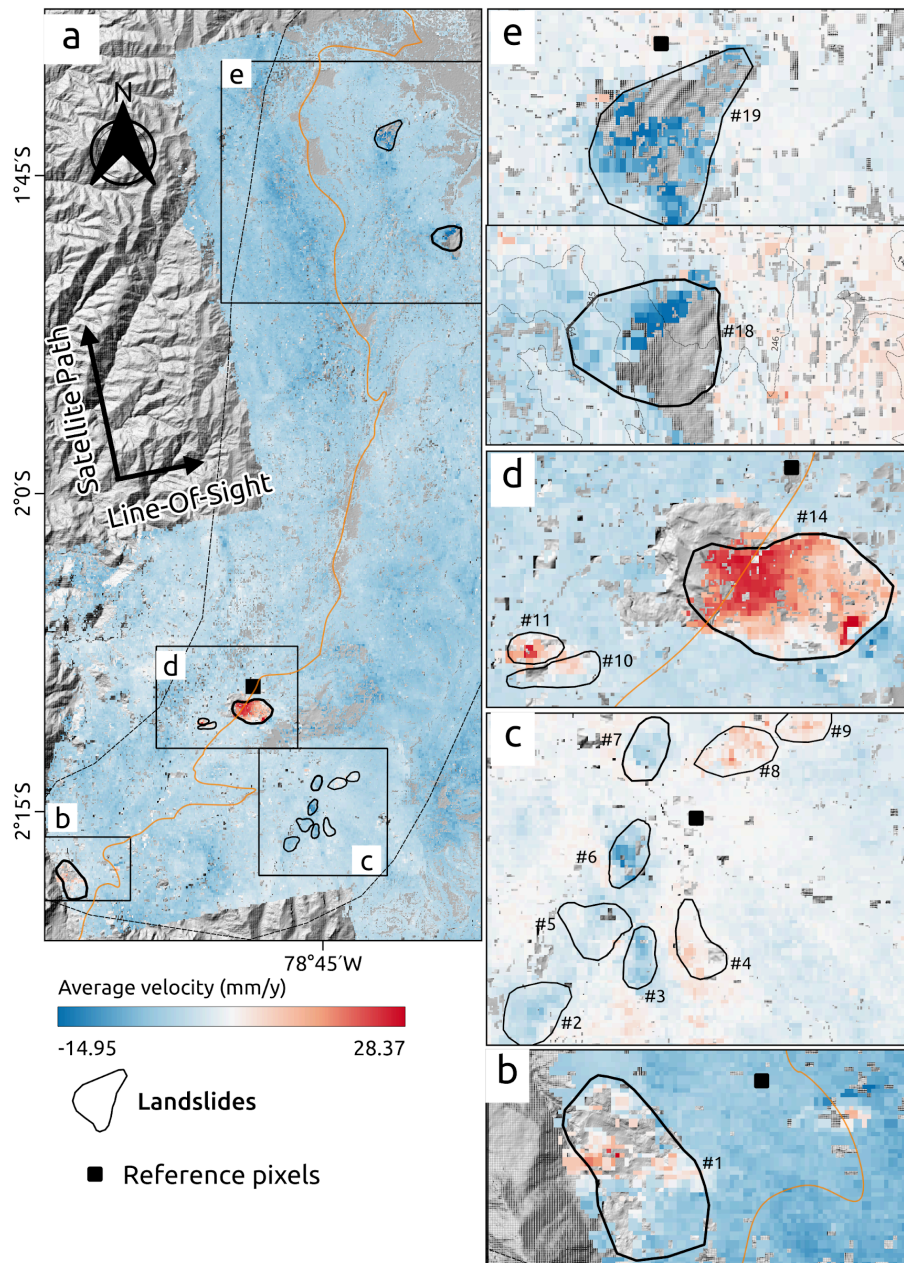


Figure 2: InSAR velocity averages for landslides during 2007 to 2012 is shown in the LOS direction along satellites ascending orbit. The color scale bar indicates negative and positive values related to LOS direction. a) highlights high, localized, landslide velocity against the background velocity. b), c), d), and e) show average velocity with respect to new reference pixels.

Realizado por: Javier Lima

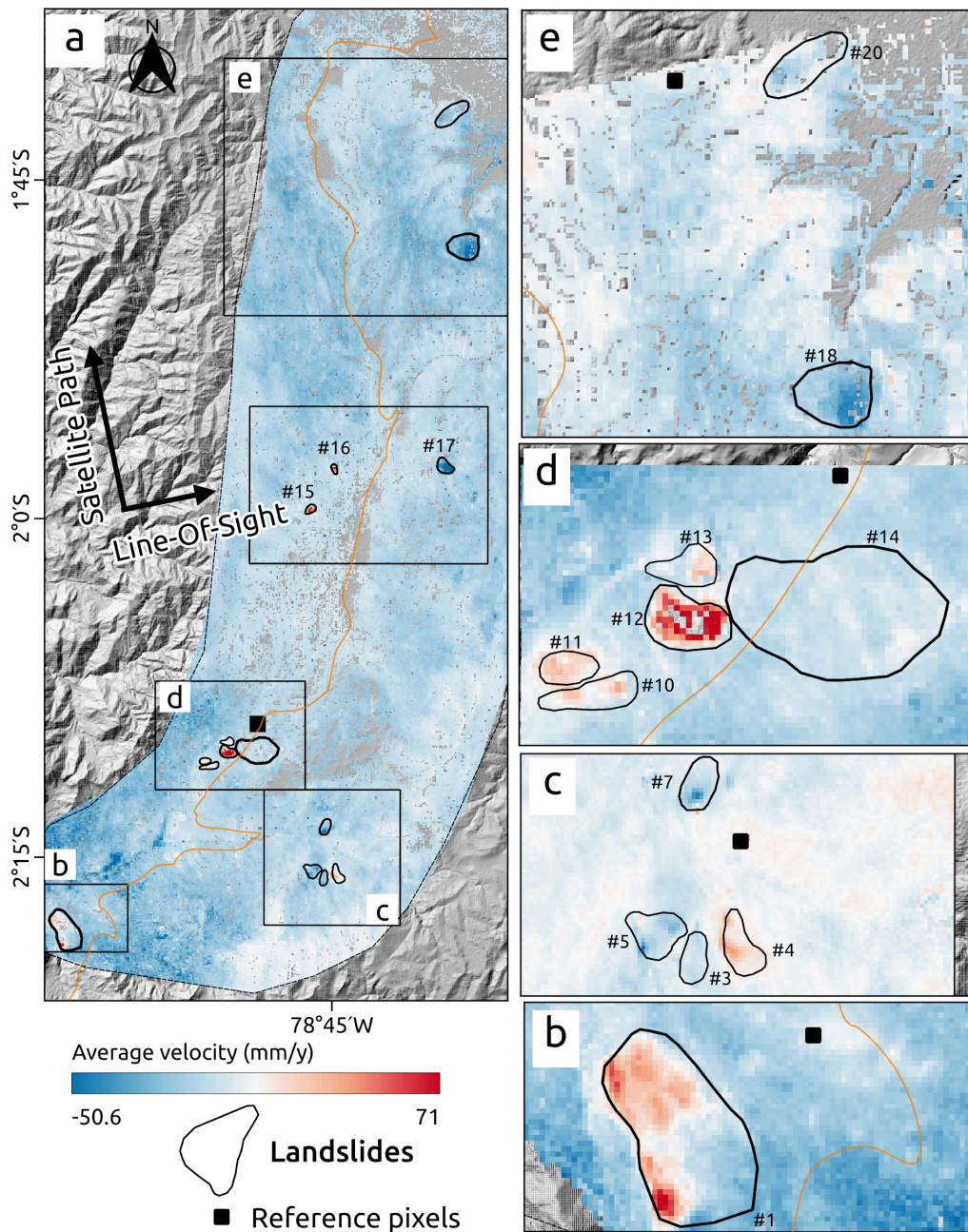


Figure 3: InSAR velocity averages for landslides during 2016 to 2022 are shown in the LOS direction along satellites ascending orbit. The color scale bar indicates negative and positive values related to LOS direction. a) highlights high, localized, landslide velocity against the background velocity. b), c), d), and e) show average velocity with respect to new reference pixels.

Realizado por: Javier Lima

Average velocity from 2007 to 2011 for landslides #1 and #14 was 7.1 and 16.2 mm/yr respectively (Fig. 4a and 4b). From 2016 to 2022 landslides #1 and #12 show 7.6 and 26.5 mm/yr respectively (Fig. 4c and 4d), while landslide #14 does not show activity.

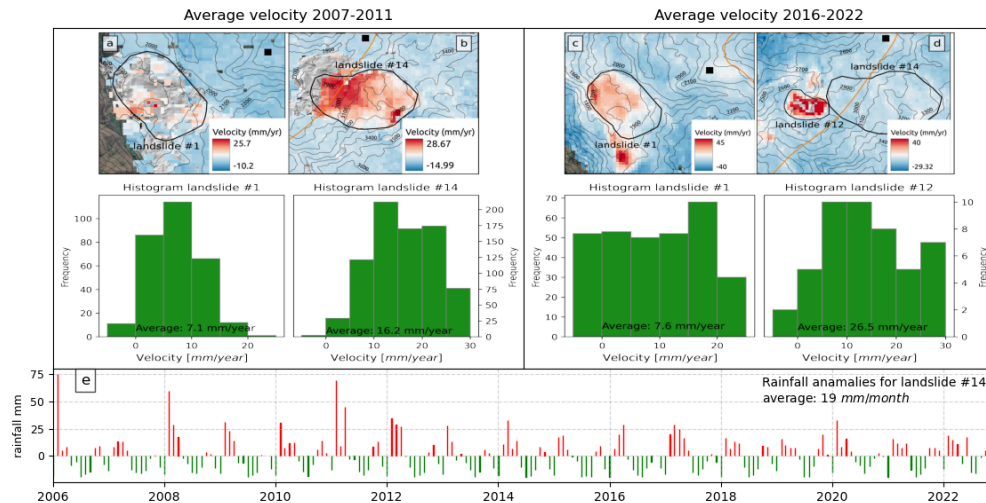


Figure 4: a-d) InSAR velocity and e) monthly rainfall anomalies for landslides #9
Realizado por: Javier Lima

In order to explain the inactivity of landslide #14 during 2016 and 2022, the monthly cumulative rainfall time series was converted into an anomaly time series (Fig. 3e) by dividing the 2006-2022 mean for each month in the monthly cumulative time series. The total cumulative rainfall from 2006 to 2011 during February and March is higher than the rest of the years, which may have triggered landslides. Landslides identified here were compared to previous landslides inventories and summarized in table 1.

Table 1: Comparison between landslides identified by InSAR in this work and previous inventories.

Landslide identified in this work	Landslides identified in previous inventories
Landslides #1 Fig 2b, 3b and #20	They are described as earth slide by La Hoja Geológica del Cantón Alausí, escala 1:100.000 (available at https://www.geoportaligm.gob.ec/portal/index.php/cartografia-de-libre-acceso-escala-50k/).
Landslide #5 Fig 2c and Fig 3c	Pacha 's landslide located in Achupallas town, Canton Alausi is a rotational landslide that was triggered by water filtration from an irrigation system in 2004. The landslide is about 400 m length, 200 width and 9 m deep (Servicio Nacional de Geología y Minería, Publicación Geológica Multinacional, 2007).
Landslide #10 Fig 2d and Fig 3d	This landslide is a debris avalanche generated in June of 1985 located in el Cantón Alausí (Eras & Plaza, 2013).
Landslide #13 Fig 3d	This landslide located in Tixan town was triggered by intense rainfall in April of 1999 (Eras & Plaza, 2013).
Landslide #19 Fig 2e	Cachas landslide (#19) was triggered by an 8.3 magnitude earthquake in 1797. It has an area of about 5km ² , a volume of 1335*10 ⁶ m ³ , and is currently active (INIGEMM , 2013).

Realizado por: Javier Lima

3.3 Pixels selection

The main aim of this work is to assess the relationship between displacement time series and rainfall time series, hence a representative-subset of displacement pixels were selected for further analysis. Pixels were selected according to the maximum cumulative displacement, therefore pixels that show cumulative displacement between percentile 75th and 98th were selected. The cumulative displacement time series for landslides #1 and #2 during 2016 to 2022 is shown in (Fig. 5).

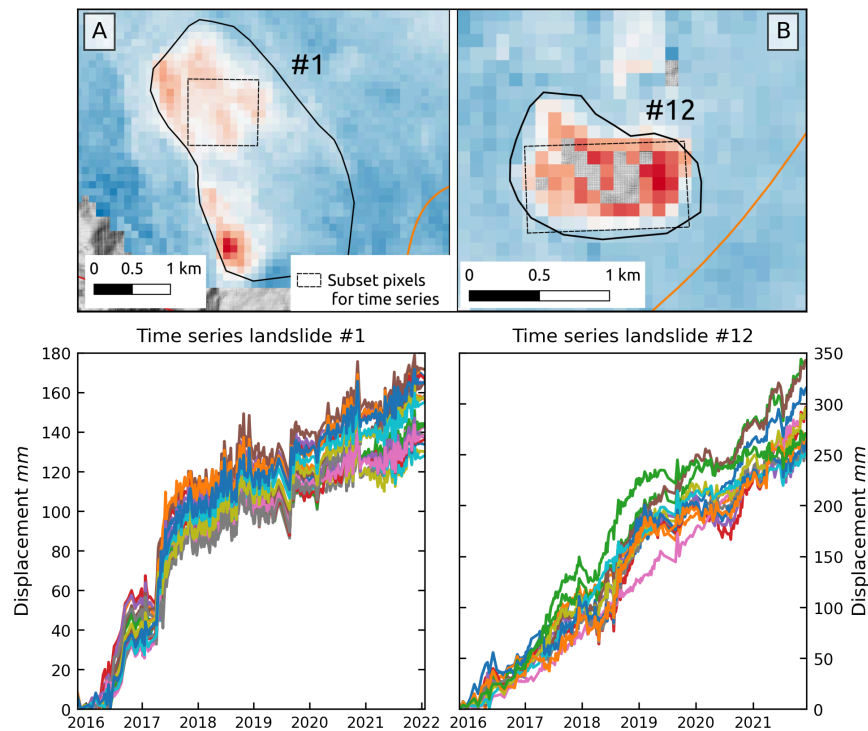


Figure 5: InSAR displacement pixels time series during 2016 to 2022.

Realizado por: Javier Lima

3.4 Continuous wavelet transform for rainfall and nonlinear term displacement time series

3.4.1 Continuous wavelet analysis for rainfall

From the continuous wavelet spectrum two different frequency events are distinguished (Fig. 6): 1) for landslide #1 a low-frequency event with high power around a

twelve-month period occurs during the whole study period (Fig. 6a) and 2) high-frequency events with an infra-annual period are observed between January and May, whereas it is less evident for 2018 and 2021. Similar patterns are absorbed for rainfall in landslide #12 (Fig. 6b).

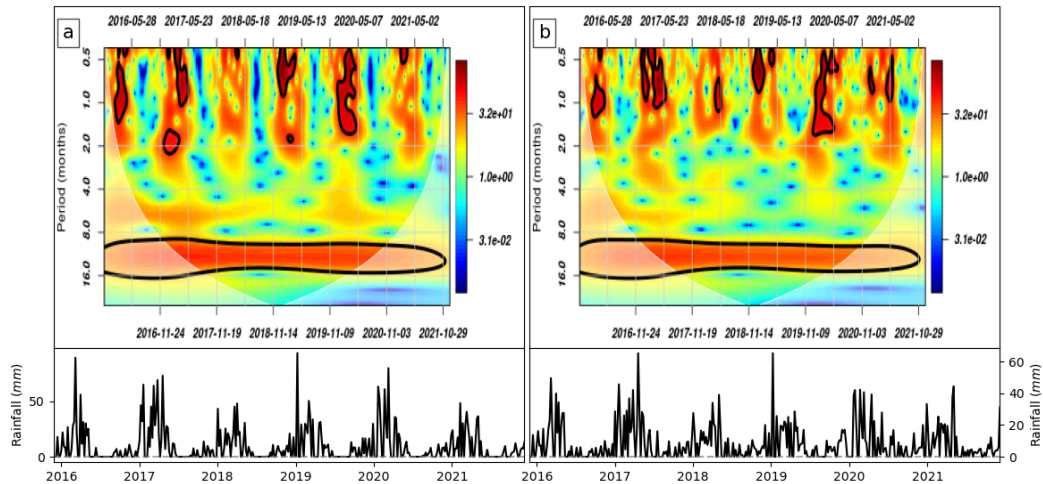


Figure 6: The continuous wavelet power of rainfall time series for landslide #1 (left) and landslide #12. The thick contour represents the 5% significance level against red noise. Area under lighter shadow represents the cone of influence (COI) where edge effects might distort the picture.

Realizado por: Javier Lima

3.4.2 Continuous wavelet analysis for displacement nonlinear term

Figure 7 presents CWT for displacement nonlinear term for landslides #1 and #12. The CWT for landslide #1 (Fig. 7a) shows a high significant power for a low-frequency event with a one-year cycle from 2016 to 2019, and infra-annual (period < months) events are mainly clustered from June 2018 to June 2019 and 2021. The CWT of displacement nonlinear term for landslide #12 (Fig. 7b) reveals multiple periodic events: a multi-annual event in 2018, an annual event in 2020, and infra-annual events (< months) mainly clustered during 2018 and 2021.

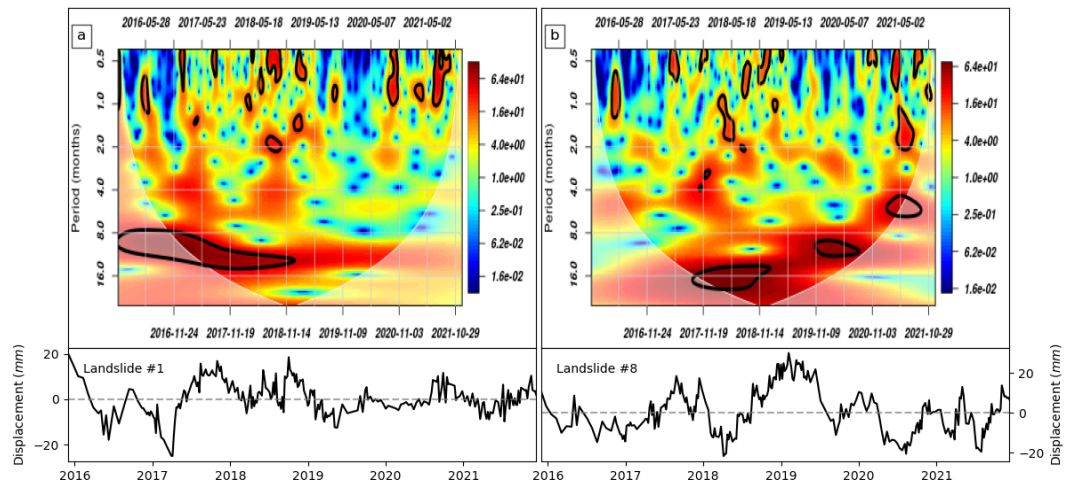


Figure 7: The continuous wavelet power of displacement nonlinear term, landslide #1 (left) and landslide #12 (right). The thick contour represents the 5% significance level against red noise. Area under lighter shadow represents the cone of influence (COI) where edge effects might distort the picture.

Realizado por: Javier Lima

3.4.3 Coherence wavelet analysis

Landslide displacement and rainfall time series are correlated in different periods (Fig 8). The WTC between displacement nonlinear component and rainfall for landslide #1 (Fig 8) shows significant coherence values for infra-annual periods (< 8 months) mainly during 2017 to 2021, a one-year period for whole study period, and a multi-annual period (> 16 months). The WTC for landslide #12 (Fig. 9) shows high coherence values for infra-annual periods during November 2018 to June 2020, annual, and multi-annual structures present moderate coherence values.

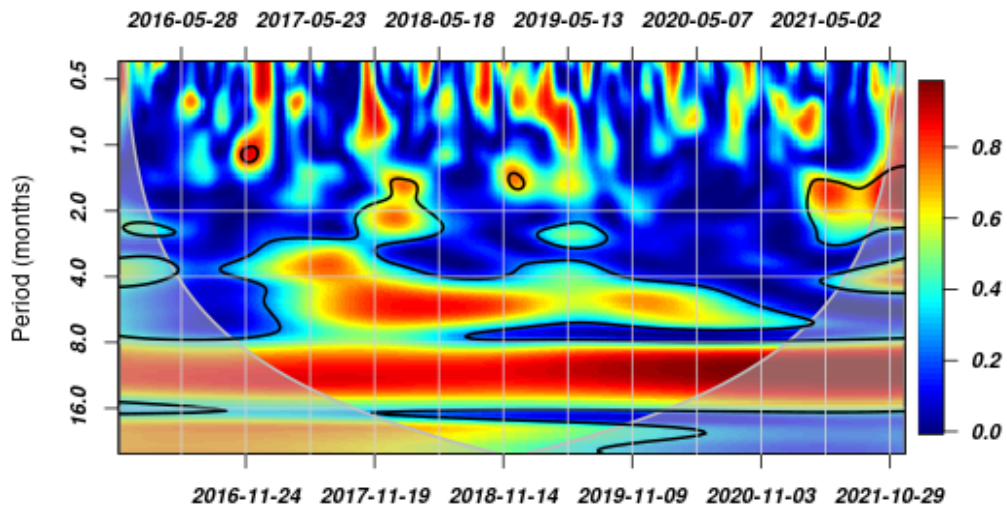


Figure 8: Wavelet coherence spectra between rainfall and displacement nonlinear term for landslide #1 The thick contour represents the 5% significance level against red noise. Area under lighter shadow represents the cone of influence (COI) where edge effects might distort the picture.

Realizado por: Javier Lima

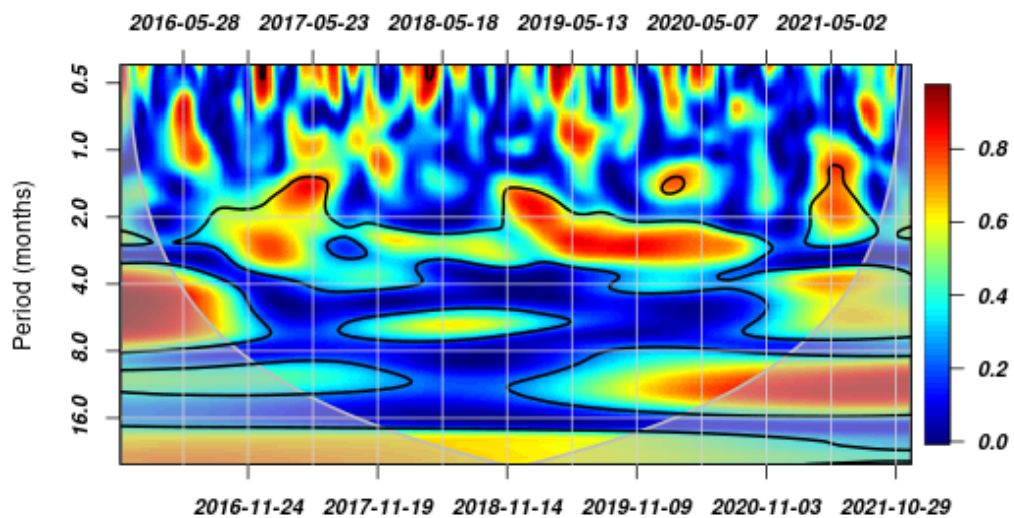


Figure 9: Wavelet coherence spectra between rainfall and displacement nonlinear term for landslide #12 The thick contour represents the 5% significance level against red noise. Area under lighter shadow represents the cone of influence (COI) where edge effects might distort the picture.

Realizado por: Javier Lima

4. DISCUSSION

4.1 InSAR limitation

In this section the limitation of InSAR to identify landslides is discussed. In total 20 landslides were identified in both periods 2007-2011 and 2016-2022 by only ascending orbits either for ALOS/PALSAR-1 or Sentinel 1AB. Landslides #1, #5, #10, #13, #19 and #20 have been described by (Eras & Plaza, 2013) and (INIGEMM, 2013) table 1. In the ascending orbit (satellite flying southeast to northwest), the sensor is more sensitive measuring the deformation on eastward slopes, therefore landslides in westward-facing slopes cannot be detected (Wasowski & Bovenga, 2014; Zhao et al., 2012). Additionally, InSAR sensors are less sensitive to slides moving parallel to the satellite flight direction, which means that nine-degree northwest slopes might not be detected (Zhao et al., 2012).

Although L-band ALOS/PALSAR-1 SAR images were used from 2007 to 2011 to minimize the effects of temporal decorrelation over vegetated areas, landslides that could be located in areas of extremely dense vegetation might not be mapped.

4.2 Relationship between InSAR displacement and rainfall

The CWT was used to expand the time series from the time domain to the time-frequency space, which allows us to analyze how time series frequency components change over time (Kumar & Foufoula-Georgio, 1997). The two seasonalities in rainfall time series are shown by the CWT (Fig. 5). This finding agrees with spatial rainfall patterns over the IAD described by (Vuille et al., 2000), where due to the influence of the west air masses from the Pacific Ocean and the east by the Amazon watershed the IAD is characterized by two rainy seasons (February–May and October–November).

Figure 7. exposes that landslide displacement and rainfall are correlated in multiple periods. The significant values of coherence along infra-annual period (< 2 months) for #1 and #8 suggest that both landslides are sensitive to high rainfall events. Massey et al. (2013) described fast displacement events in deep-seated landslides are originated by basal sliding and triggered by long periods (12 to 18 weeks) of rainfall.

Correlation in an annual and multi annual periods for landslides #1 and #12 suggest that a continuous, slow, creep-like landslide movement might be related to slip on the slide base and plastic deformation within the landslide body described by Massey et al. (2013) and Petley & Allison (1997), or ground water process (Vallet et al., 2016).

5. CONCLUSION

This work aimed to identify landslides by InSAR time series analysis and correlate landslide displacement with rainfall dynamics in the Inter-Andean Depression. Twenty landslides were identified, and three of them were analyzed because they were close to the Pan-American highway or human settlement. Landslide #14 average velocity was 16 mm/year in the LOS direction during 2007 and 2011, while for the period 2016 to 2022, it did not show activity. Landslides #1 and #2 average velocities were 7.6 and 26.5 mm/year respectively in the LOS direction during 2016 to 2022. The wavelet analysis of landslide displacement time series for landslides #1 and #12 showed that landslides displacement correlates with rainfall in infra-annual, annual, and multi-annual periods. The patterns in landslide displacement might be explained by high rainfall events and processes related to landslide soil mechanisms.

6. BIBLIOGRAPHY

- Alvarado, A., Audin, L., Nocquet, J. M., Jaillard, E., Mothes, P., Jarrín, P., Segovia, M., Rolandone, F., & Cisneros, D. (2016). Partitioning of oblique convergence in the Northern Andes subduction zone: Migration history and the present-day boundary of the North Andean Sliver in Ecuador. *Tectonics*, *35*(5), 1048–1065.
- Baize, S., Audin, L., Alvarado, A., Jomard, H., Bablon, M., Champenois, J., Espin, P., Samaniego, P., Quidelleur, X., & Le Pennec, J.-L. (2020). Active Tectonics and Earthquake Geology Along the Pallatanga Fault, Central Andes of Ecuador. *Frontiers of Earth Science in China*, *8*. <https://doi.org/10.3389/feart.2020.00193>
- Bekaert, D. P. S., Handwerger, A. L., Agram, P., & Kirschbaum, D. B. (2020). InSAR-based detection method for mapping and monitoring slow-moving landslides in remote regions with steep and mountainous terrain: An application to Nepal. *Remote Sensing of Environment*, *249*, 111983.
- Berardino, P., Fornaro, G., Lanari, R., & Sansosti, E. (2002). A new algorithm for surface deformation monitoring based on small baseline differential SAR interferograms. *IEEE Transactions on Geoscience and Remote Sensing: A Publication of the IEEE Geoscience and Remote Sensing Society*, *40*(11), 2375–2383.
- Bogaard, T. A., & Greco, R. (2016). Landslide hydrology: from hydrology to pore pressure. *WIREs. Water*, *3*(3), 439–459.
- Bucci, F., Santangelo, M., Cardinali, M., Fiorucci, F., & Guzzetti, F. (2016). Landslide distribution and size in response to Quaternary fault activity: the Peloritani Range, NE Sicily, Italy. *Earth Surface Processes and Landforms*, *41*(5), 711–720.
- Bürgmann, R., Rosen, P. A., & Fielding, E. J. (2000). Synthetic Aperture Radar Interferometry to Measure Earth's Surface Topography and Its Deformation. *Annual Review of Earth and Planetary Sciences*, *28*(1), 169–209.
- Buzzanga, B., Bekaert, D. P. S., Hamlington, B. D., & Sangha, S. S. (2020). Toward sustained monitoring of subsidence at the coast using InSAR and GPS: An application in Hampton roads, Virginia. *Geophysical Research Letters*, *47*(18). <https://doi.org/10.1029/2020gl090013>
- Casagli, N., Intrieri, E., Tofani, V., Gigli, G., & Raspini, F. (2023). Landslide detection, monitoring and prediction with remote-sensing techniques. *Nature Reviews Earth & Environment*, *4*(1), 51–64.
- Champenois, J., Baize, S., Vallee, M., Jomard, H., Alvarado, A., Espin, P., Ekström, G., & Audin, L. (2017). Evidences of surface rupture associated with a low-magnitude (M_w 5.0) shallow earthquake in the

- Ecuadorian Andes. *Journal of Geophysical Research, [Solid Earth]*, 122(10), 8446–8458.
- Cohen-Waeber, J., Bürgmann, R., Chaussard, E., Giannico, C., & Ferretti, A. (2018). Spatiotemporal patterns of precipitation-modulated landslide deformation from independent component analysis of InSAR time series. *Geophysical Research Letters*, 45(4), 1878–1887.
- Corominas, J., Moya, J., Ledesma, A., Lloret, A., & Gili, J. A. (2005). Prediction of ground displacements and velocities from groundwater level changes at the Vallcebre landslide (Eastern Pyrenees, Spain). *Landslides*, 2(2), 83–96.
- Crespo, P. J., Feyen, J., Buytaert, W., Bücker, A., Breuer, L., Frede, H.-G., & Ramírez, M. (2011). Identifying controls of the rainfall–runoff response of small catchments in the tropical Andes (Ecuador). *Journal of Hydrology*, 407(1), 164–174.
- Eras, M., & Plaza, G. (2013). MAPA DE SUSCEPTIBILIDAD POR MOVIMIENTOS EN MASA DEL ECUADOR, ESCALA 1:1'000.000 (VERSIÓN PRELIMINAR). INSTITUTO NACIONAL DE INVESTIGACIÓN GEOLÓGICO MINERO METALÚRGICO. https://iedg.sni.gob.ec/wp-content/uploads/2022/09/IIGE_IT3_Mapa_Susceptibilidad_Escala_1M_2013.pdf
- Fattahi, H., Simons, M., & Agram, P. (2017). InSAR Time-Series Estimation of the Ionospheric Phase Delay: An Extension of the Split Range-Spectrum Technique. *IEEE Transactions on Geoscience and Remote Sensing: A Publication of the IEEE Geoscience and Remote Sensing Society*, 55(10), 5984–5996.
- Ferretti, A., Monti-Guarnieri, A., Prati, C., & Rocca, F. (2007). *InSAR Principles: Guidelines for SAR Interferometry Processing and Interpretation (ESA TM-19)* (K. Fletcher (ed.)). ESA Publications.
- Froude, M. J., & Petley, D. N. (2018). Global fatal landslide occurrence from 2004 to 2016. *Natural Hazards and Earth System Sciences*, 18(8), 2161–2181.
- Funk, C. C., Peterson, P. J., Landsfeld, M. F., Pedreros, D. H., Verdin, J. P., Rowland, J. D., Romero, B. E., Husak, G. J., Michaelsen, J. C., & Verdin, A. P. (2014). *A Quasi-Global Precipitation Time Series for Drought Monitoring* (832). U.S. Geological Survey. <https://pubs.usgs.gov/ds/832/>
- Gregg, P. M., Zhan, Y., Amelung, F., Geist, D., Mothes, P., Koric, S., & Yunjun, Z. (2022). Forecasting mechanical failure and the 26 June 2018 eruption of Sierra Negra Volcano, Galápagos, Ecuador. *Science Advances*, 8(22), eabm4261.
- Grinsted, A., Moore, J. C., & Jevrejeva, S. (2004). Application of the cross wavelet transform and wavelet coherence to geophysical time series. *Nonlinear Processes in Geophysics*, 11(5/6), 561–566.
- Handwerger, A. L., Fielding, E. J., Sangha, S. S., & Bekaert, D. P. S. (2022). Landslide Sensitivity and Response to Precipitation Changes in Wet and Dry Climates. *Geophysical Research Letters*,

49(13), e2022GL099499.

- Handwerger, A. L., Huang, M.-H., Fielding, E. J., Booth, A. M., & Bürgmann, R. (2019). A shift from drought to extreme rainfall drives a stable landslide to catastrophic failure. *Scientific Reports*, *9*(1), 1569.
- Handwerger, A. L., Roering, J. J., & Schmidt, D. A. (2013). Controls on the seasonal deformation of slow-moving landslides. *Earth and Planetary Science Letters*, *377-378*, 239–247.
- Hanssen, R. F. (2001). *Radar Interferometry Data Interpretation and Error Analysis*. Springer Netherlands.
- Hendron, A. J., & Patton, F. D. (1987). The vaiont slide — A geotechnical analysis based on new geologic observations of the failure surface. *Engineering Geology*, *24*(1), 475–491.
- Hilley, G. E., Bürgmann, R., Ferretti, A., Novali, F., & Rocca, F. (2004). Dynamics of slow-moving landslides from permanent scatterer analysis. *Science*, *304*(5679), 1952–1955.
- Hungr, O., Leroueil, S., & Picarelli, L. (2014). The Varnes classification of landslide types, an update. *Landslides*, *11*(2), 167–194.
- INIGEMM, (2013). Memoria Técnica Ensayos Metodológicos para la Zonificación de la Susceptibilidad/ Amenaza por Movimientos en Masa, Zona de Riobamba.
- Kumar, P., & Fofoula-Georgio, E. (1997). Wavelet analysis for geophysical applications. *Reviews of Geophysics*, *35*. <https://doi.org/10.1029/97RG00427>
- Lau, K.-M., & Weng, H. (1995). Climate Signal Detection Using Wavelet Transform: How to Make a Time Series Sing. *Bulletin of the American Meteorological Society*, *76*(12), 2391–2402.
- Liu, X., Zhao, C., Zhang, Q., Lu, Z., Li, Z., Yang, C., Zhu, W., Liu-Zeng, J., Chen, L., & Liu, C. (2021). Integration of Sentinel-1 and ALOS/PALSAR-2 SAR datasets for mapping active landslides along the Jinsha River corridor, China. *Engineering Geology*, *284*, 106033.
- Lu, Z., Dzurisin, D., Jung, H.-S., Zhang, J., & Zhang, Y. (2010). Radar image and data fusion for natural hazards characterisation. *International Journal of Image and Data Fusion*, *1*(3), 217–242.
- Mackey, B. H., & Roering, J. J. (2011). Sediment yield, spatial characteristics, and the long-term evolution of active earthflows determined from airborne LiDAR and historical aerial photographs, Eel River, California. *GSA Bulletin*, *123*(7-8), 1560–1576.
- Mackey, B. H., Roering, J. J., & McKean, J. A. (2009). Long-term kinematics and sediment flux of an active earthflow, Eel River, California. *Geology*, *37*(9), 803–806.
- Massey, C. I., Petley, D. N., & McSaveney, M. J. (2013). Patterns of movement in reactivated landslides. *Engineering Geology*, *159*, 1–19.
- Massonnet, D., Rossi, M., Carmona, C., Adragna, F., Peltzer, G., Feigl, K., & Rabaute, T. (1993). The displacement field of the Landers earthquake mapped by radar interferometry. *Nature*, *364*(6433),

138–142.

- Nappo, N., Peduto, D., Mavrouli, O., van Westen, C. J., & Gullà, G. (2019). Slow-moving landslides interacting with the road network: Analysis of damage using ancillary data, in situ surveys and multi-source monitoring data. *Engineering Geology*, *260*, 105244.
- Nocquet, J.-M., Villegas-Lanza, J. C., Chlieh, M., Mothes, P. A., Rolandone, F., Jarrin, P., Cisneros, D., Alvarado, A., Audin, L., Bondoux, F., Martin, X., Font, Y., Régnier, M., Vallée, M., Tran, T., Beauval, C., Maguiña Mendoza, J. M., Martinez, W., Tavera, H., & Yepes, H. (2014). Motion of continental slivers and creeping subduction in the northern Andes. *Nature Geoscience*, *7*(4), 287–291.
- Petley, D. N., & Allison, R. J. (1997). The mechanics of deep-seated landslides. *Earth Surface Processes and Landforms*, *22*(8), 747–758.
- Rosen, P. A., Gurrola, E., Sacco, G. F., & Zebker, H. (2012). The InSAR scientific computing environment. *EUSAR 2012; 9th European Conference on Synthetic Aperture Radar*, 730–733.
- Servicio Nacional de Geología y Minería, Publicación Geológica Multinacional. (2007). Proyecto Multinacional Andino: Geociencias para las Comunidades Andinas (2007). Movimientos en Masa en la Región Andina: Una guía para la evaluación de amenazas (4). Servicio Nacional de Geología y Minería (Chile). <https://repositorio.ingemmet.gob.pe/handle/20.500.12544/2830>
- Scheingross, J. S., Minchew, B. M., Mackey, B. H., Simons, M., Lamb, M. P., & Hensley, S. (2013). Fault-zone controls on the spatial distribution of slow-moving landslides. *GSA Bulletin*, *125*(3-4), 473–489.
- Schulte, J. A. (2019). Statistical hypothesis testing in wavelet analysis: theoretical developments and applications to Indian rainfall. *Nonlinear Processes in Geophysics*, *26*(2), 91–108.
- Schuster, R. L., NietoThomas, A. S., D. O'Rourke, T., Crespo, E., & Plaza-Nieto, G. (1996). Mass wasting triggered by the 5 March 1987 Ecuador earthquakes. *Engineering Geology*, *42*(1), 1–23.
- Simons, M., & Rosen, P. A. (2007). 3.12 - Interferometric Synthetic Aperture Radar Geodesy. In G. Schubert (Ed.), *Treatise on Geophysics* (pp. 391–446). Elsevier.
- Soralump, S., Shrestha, A., Thowiwat, W., Sukjaroen, R., Chaithong, T., Yangsanphu, S., Koirala, A., & Jotisankasa, A. (2021). Assessment of landslide behaviour in colluvium deposit at Doi Chang, Thailand. *Scientific Reports*, *11*(1), 22960.
- Soto, J., Galve, J. P., Palenzuela, J. A., Azañón, J. M., Tamay, J., & Irigaray, C. (2017). A multi-method approach for the characterization of landslides in an intramontane basin in the Andes (Loja, Ecuador). *Landslides*, *14*(6), 1929–1947.
- Styron, R., & Pagani, M. (2020). The GEM Global Active Faults Database. *Earthquake Spectra*,

36(1_suppl), 160–180.

- Tarik C, Grinsted A, Simko V. R package biwavelet: Conduct Univariate and Bivariate Wavelet Analyses. Github; 2018. Available: <https://github.com/tgouhier/biwavelet>
- Temple, P. H., & Rapp, A. (1972). Landslides in the Mgeta Area, Western Uluguru Mountains, Tanzania. *Geografiska Annaler: Series A, Physical Geography*, 54(3-4), 157–193.
- Tomás, R., Li, Z., Lopez-Sanchez, J. M., Liu, P., & Singleton, A. (2016). Using wavelet tools to analyse seasonal variations from InSAR time-series data: a case study of the Huangtupo landslide. *Landslides*, 13(3), 437–450.
- Torrence, C., & Compo, G. P. (1998). A Practical Guide to Wavelet Analysis. *Bulletin of the American Meteorological Society*, 79(1), 61–78.
- Vallet, A., Charlier, J. B., Fabbri, O., Bertrand, C., Carry, N., & Mudry, J. (2016). Functioning and precipitation-displacement modelling of rainfall-induced deep-seated landslides subject to creep deformation. *Landslides*, 13(4), 653–670.
- Varnes, D. (1978). *Slope Movement Types and Processes* (176). Transportation research board, National Academy of Sciences, Washington, DC. [https://www.scirp.org/\(S\(czeh2tfqyw2orz553k1w0r45\)\)/reference/ReferencesPapers.aspx?ReferenceID=1855370](https://www.scirp.org/(S(czeh2tfqyw2orz553k1w0r45))/reference/ReferencesPapers.aspx?ReferenceID=1855370)
- Vasconez, F., Pacheco, D., Viracucha, C., Toro, M., Córdova, A., Saqui, D., & Ruiz, M. (2023). *OBSERVACIONES SOBRE EL DESLIZAMIENTO DEL 26 DE MARZO DE 2023 EN ALAUSÍ (PROVINCIA DE CHIMBORAZO)*. Instituto Geofísico Escuela Politécnica Nacional. https://www.igepon.edu.ec/portal/informes/otros/deslizamiento_alausi.pdf
- Vuille, M., Bradley, R. S., & Keimig, F. (2000). Climate Variability in the Andes of Ecuador and Its Relation to Tropical Pacific and Atlantic Sea Surface Temperature Anomalies. *Journal of Climate*, 13(14), 2520–2535.
- Wasowski, J., & Bovenga, F. (2014). Investigating landslides and unstable slopes with satellite Multi Temporal Interferometry: Current issues and future perspectives. *Engineering Geology*, 174, 103–138.
- Yunjun, Z., Fattahi, H., & Amelung, F. (2019). Small baseline InSAR time series analysis: Unwrapping error correction and noise reduction. *Computers & Geosciences*, 133, 104331.
- Zebker, H. A., & Villasenor, J. (1992). Decorrelation in Interferometric Radar Echoes. *IEEE Transactions on Geoscience and Remote Sensing*. <https://doi.org/10.1109/36.175330>
- Zhao, C., Lu, Z., Zhang, Q., & de la Fuente, J. (2012). Large-area landslide detection and monitoring with ALOS/PALSAR imagery data over Northern California and Southern Oregon, USA. *Remote*

Sensing of Environment, 124, 348–359.